Nanostructures

DOI: 10.1002/anie.200602228

SiO_2/Ta_2O_5 Core–Shell Nanowires and Nanotubes**

Yu-Lun Chueh, Li-Jen Chou, and Zhong Lin Wang*

One-dimensional nanostructures such as nanowires, nanobelts, and nanotubes have attracted much attention as a result of their unique properties, which can be applied in the fabrication of biomedical sensors, optoelectronic devices, field-effect transistors, and field-emission devices, for example.[1] In particular, one-dimensional nanostructures of metal oxides such as ZnO,[2] SnO_2,[3] α-Fe_2O_3,[4] WO_3,[5] and Ta_2O_5,[6] so-called functional materials, have been widely studied. The synthesis of these functional metal oxide nanostructures are investigated widely through physical and chemical reactions, including vapor–liquid–solid (VLS),[7] solution–liquid–solid (SLS),[8] vapor–solid (VS),[9] and other template-based approaches.[10]

Ta_2O_5 is a fascinating functional material that has been used in applications such as dynamic random access memory (DRAM) devices, antireflection coating layers, gas sensors, photocatalysts, and capacitors owing to its high dielectric constant, high refractive index, chemical stability, and high-temperature piezoelectric properties.[6a,11] However, the synthesis of Ta_2O_5 nanostructures (e.g. nanowires or nanotubes) has had little success as a result of its high melting point. On the other hand, silica (SiO_2) nanowires are well developed for electronic and optoelectronic applications.[12] Various methods of synthesizing SiO_2 nanowires include pulsed laser ablation,[12a] directed growth from a silica substrate or silica nanoparticles in a reductive atmosphere,[13] direct growth from a Si substrate with catalyst,[14] carbon-assisted and carbothermal reduction of silicon dioxide or metal oxides,[15] and the sol–gel method.[16] All of these approaches are direct, simple, and high-yielding, which are important factors for commercial applications.

[*] Y.-L. Chueh, Prof. L.-J. Chou
Department of Materials Science and Engineering
National Tsing Hua University
Hsinchu, Taiwan 300 (ROC)
Fax: (+886) 3-572-2366
E-mail: ljchou@mx.nthu.edu.tw
Y.-L. Chueh, Prof. Z. L. Wang
School of Materials Science and Engineering
Georgia Institute of Technology
Atlanta, Georgia 30332-0245 (USA)

[**] This research was supported by the National Science Council (grant no. NSC 94-2215-E-007-019), the Ministry of Education (grant no. 93-E-FA04-1-4), the Thousand Horse Program (no. 095-2917-1-007-014), the NSF, the NASA Vehicle System Program, the Department of Defense Research and Engineering (DDR&E), and the Defense Advanced Research Project Agency (N66001-040-1-18903).

Supporting information for this article is available on the WWW under http://www.angewandte.org or from the author.

Herein, we present a technique for the fabrication of SiO_2/Ta_2O_5 core–shell nanotubes, Ta_2O_5 nanotubes, and Ta_2O_5 nanowires by using SiO_2 nanowires as template. The structures were prepared by annealing SiO_2 nanowires in an atmosphere of Ta at 950 °C at a pressure of 1×10^{-6} Torr. The diameter of the SiO_2 core in the SiO_2/Ta_2O_5 core–shell structure was readily controlled, and the silica template could be removed from the core–shell structures by using dilute HF solution to leave Ta_2O_5 nanotubes. Furthermore, Ta_2O_5 nanowires could be synthesized by increasing the reduction (annealing) time so that all of the SiO_2 in the core–shell structure was reduced by Ta vapors. The subsequent characterization of the core–shell structures as well as the Ta_2O_5 nanotubes and nanowires was carried out by cathodoluminescence (CL) and field-emission measurements.

The scanning electron microscopy (SEM) image of SiO_2 nanowires, prepared by annealing a 2-nm-thick layer of Au on a Si wafer under N_2 atmosphere at 1150 °C for 2 h, is shown in Figure 1 a. The diameter of these SiO_2 nanowires is almost uniform, and the length is up to several hundred micrometers. The corresponding transmission electron microscopy (TEM) image indicates that most of the SiO_2 nanowires have a smooth morphology, with a diameter of 100–150 nm (Figure 1 b). The diffraction pattern (upper inset in Figure 1 b) displays a highly diffusive ring, indicating that the silica nanowires are amorphous. The atomic concentration of Si and O for these synthesized nanowires is about 34 % and 66 %, respectively, and a ratio of 1:2 Si/O was inferred from quantitative TEM/EDS (energy-dispersive spectrometry) measurements (lower inset in Figure 1 b). After annealing the nanowires at 950 °C for 12 h and subjecting them to a reductive Ta atmosphere, the morphology of the resultant SiO_2/Ta_2O_5 structures was similar (Figure 1 c). The corresponding magnified SEM image (upper inset in Figure 1 c) clearly shows the wirelike features. The phase and structure of these nanowires was characterized by X-ray diffraction (XRD; Figure 1 d) and revealed the Ta_2O_5 phase to have an orthorhombic structure (*C*2*mm* space group) and lattice constants of $a = 0.618$, $b = 0.366$, and $c = 0.388$ nm, respectively (ICSD-43498).[17] Note that the $TaSi_2$ phase found in the XRD spectrum originates from a silicide reaction between the Si substrate and Ta vapors during the reduction procedure.

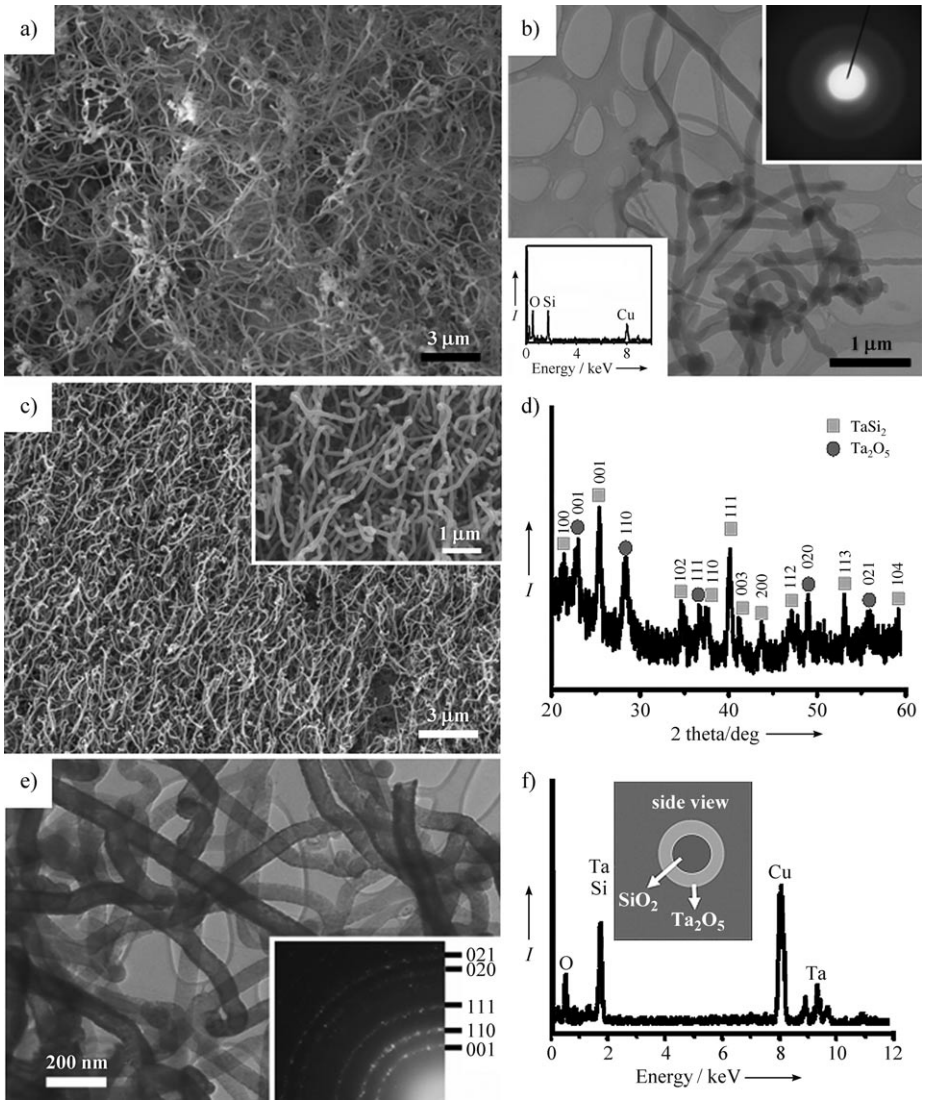

Figure 1. a) Top-view SEM image and b) corresponding TEM image of SiO_2 nanowires. The upper inset in (b) shows an electron diffraction pattern from a nanowire, while the lower inset shows the EDS spectrum. c) Top-view SEM image of SiO_2/Ta_2O_5 core–shell nanostructures formed by annealing SiO_2 nanowires under a Ta atmosphere at 950 °C for 12 h. The inset in (c) shows the magnified SEM image. d) XRD spectrum corresponding to the sample in (c). e) TEM image of SiO_2/Ta_2O_5 core–shell nanostructures. The inset in (e) shows the diffraction pattern. f) EDS spectrum recorded on the Ta_2O_5 shell of a SiO_2/Ta_2O_5 nanostructure and schematic of the configuration of the core–shell nanostructure.

TEM analysis was essential to examine the detailed microstructures of these nanowires (Figure 1 e). The different contrast between the inside and the outside of these nanowires provides significant evidence of a core–shell structure. The lower inset in Figure 1 e shows the diffraction pattern and plane indices recorded from a SiO_2/Ta_2O_5 core–shell structure. The pattern is consistent with the results of XRD studies, indicating the polycrystalline characteristic of the SiO_2/Ta_2O_5 core–shell structure (see the Supporting Information). Diffusive white contrast was also observed confirming that SiO_2

nanowires were surrounded by a Ta_2O_5 shell. Note that SiO_2 or Si is incorporated inside the Ta_2O_5 shell during the reduction process, but the main phase remains that of Ta_2O_5 as determined by both the XRD and diffraction patterns (Figure 1d and e, respectively). TEM/EDS measurements of the shell of a SiO_2/Ta_2O_5 structure revealed that it consists of 20% Ta, 71% O, and 9% Si. Upon examining in detail many SiO_2/Ta_2O_5 core–shell structures, the maximum concentration of Si in these Ta_2O_5 shells was found to be no more than 15%.

The morphology of the core–shell structure was tunable, depending on the original shape of the SiO_2 nanowire. If the SiO_2 nanowire had a spiral morphology, the SiO_2/Ta_2O_5 core–shell structure formed after the reduction process also revealed a spiral morphology. An example of the spiral morphology of a SiO_2/Ta_2O_5 core–shell structure is highlighted in Figure 2a (see also the Supporting Information), while the corresponding TEM image is shown in Figure 2b. The phase was confirmed to be that of Ta_2O_5 by the diffraction pattern (see inset in Figure 2b). The thickness of the Ta_2O_5 layer outside the SiO_2 nanowires could be tuned by controlling the annealing (reduction) time (see Supporting Information). The thickness of the Ta_2O_5 shell increased as the reduction time was increased at a constant temperature of 950°C or simply if the temperature was increased.

How do the Ta atoms reduce the SiO_2 to form the SiO_2/Ta_2O_5 core–shell structure? Figure 2c shows the heat of formation ($-\Delta H_f$ [kcal atom^{-1}]) per oxygen atom for various transition-metal oxides and SiO_2.[18] Note that the heats of formation for transition-metal oxides such as HfO_2, TiO_2, and Ta_2O_5 are lower than that of SiO_2, which results in the reduction of SiO_2 at high annealing temperatures. On the other hand, the reduction of SiO_2 is prohibited if the heat of formation of transition-metal oxides such as MnO_3 is higher than that of SiO_2. Figure 2d shows plots of the thickness of the Ta_2O_5 shell of the SiO_2/Ta_2O_5 core–shell structure as a function of the reduction time at 950°C. The relationship between the thickness of the Ta_2O_5 shell and the reduction time is nonlinear, revealing that the reduction mechanism is under diffusion control, that is, $X^2 = Dt$ (X, D, and t denote the oxide thickness, parabolic reduction rate constant, and reduction time, respectively).[19] The reduction rate constant, D, was evaluated as about 2×10^{-16} cm^{2}s^{-1} by plotting the thickness of the oxide shell as a function of the square root of the reduction time (see inset in Figure 2d). The thermal kinetic motion of Ta ions during the reduction process involves their diffusion through SiO_2 and reduction of the SiO_2 layer. The diffusion-limited mechanism indicates that the diffusion through the SiO_2 layer is rather slow, resulting in easier control over the reduction process. The measured rate constant represents the rate constant of diffusion. Also, the Si signal detected in EDS studies in various Ta_2O_5 shells indicates that the Si atoms from SiO_2 reduced by Ta vapors are involved in the Ta_2O_5 sublattice or excluded from the grain boundary.

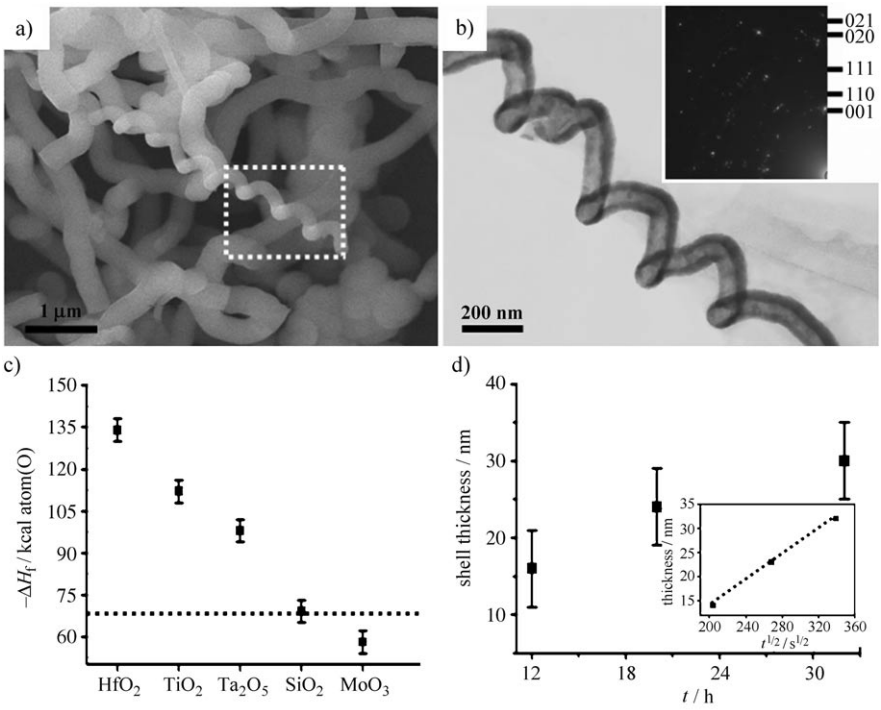

Figure 2. a) SEM image of a spiral SiO_2/Ta_2O_5 core–shell nanostructure obtained by annealing SiO_2 nanowires in a Ta atmosphere at 950°C for 12 h. b) TEM image corresponding to the dashed rectangular area in (a). The inset shows the corresponding electron diffraction pattern. c) Heats of formation ($-\Delta H_f$) for different metal oxides (the dashed line is shown to compare other metal oxides with SiO_2). d) Variation in the thickness of the Ta_2O_5 shell as a function of reduction (annealing) time. The inset shows the linear relationship between the square root of reduction time and the shell thickness.

After dipping the core–shell structures in a diluted solution of HF to remove the SiO_2 inside the SiO_2/Ta_2O_5 core–shell structure, the morphology was unchanged. The inner SiO_2 nanowires could be removed to leave Ta_2O_5 nanotubes intact (see Figure 3a and Supporting Information). The residual $TaSi_2$ formed by the reduction procedure could be completely etched by HF solution. The XRD results for the nanotubes showed no peaks for $TaSi_2$ and indicate that the amorphous SiO_2 region was eliminated (see Supporting Information).[18]

Ta_2O_5 nanowires could also be prepared by increasing the reduction time of the silica nanowires. For example, after annealing SiO_2 nanowires with a diameter of less than 60 nm in a reductive Ta atmosphere at 950°C for 32 h, then Ta_2O_5 nanowires with lengths of over several hundred micrometers were formed instead of the SiO_2/Ta_2O_5 core–shell structure (Figure 3b). The TEM image of a Ta_2O_5 nanowire with a diameter of 100 nm is shown in Figure 3c and indicates the polycrystalline feature of the structure. From the quantitative EDS measurements, it can be seen that the concentration of Si is about 3–14%. Although

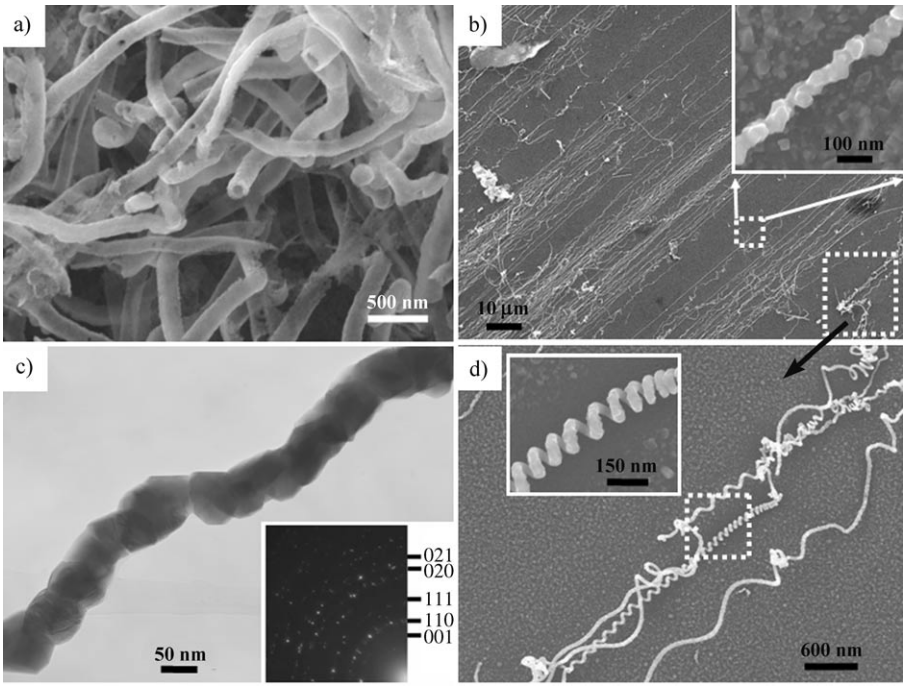

Figure 3. a) Top-view SEM image of Ta_2O_5 nanotubes prepared by dipping a sample of SiO_2/Ta_2O_5 core–shell nanostructures in diluted HF solution to remove the SiO_2 nanowire core. b) Top-view SEM image of Ta_2O_5 nanowires. The inset shows the magnified SEM image recorded from the dashed rectangle area indicated by arrows. c) Typical TEM image of a Ta_2O_5 nanowire. The inset shows the corresponding electron diffraction pattern. d) SEM image showing the spiral morphology of Ta_2O_5 nanowires taken from the larger dashed rectangular area in (b). The inset shows the magnified SEM image.

the concentration of Si inside the Ta_2O_5 nanowires is fairly high, the main phase remains that of Ta_2O_5, as confirmed by the diffraction pattern shown in the lower inset in Figure 3c. The morphology of the Ta_2O_5 nanowires could be modified according to the original morphology of the SiO_2 nanowire template (lower right inset of Figure 3b shows the spiral morphology of Ta_2O_5 nanowires). The magnified SEM image of the spiral morphology of the Ta_2O_5 nanowires as well as a magnification of this spiral structure are clearly seen in Figure 3d. The polycrystalline feature is suggested to arise as a result of two possible factors: 1) the segregation of Si during the reduction process through the grain boundary of Ta_2O_5 nanowires and 2) anisotropic reduction along the SiO_2 nanowires. Moreover, dislocations can be found inside the grain of Ta_2O_5 which may be caused by the location of Si atoms in the substitutional or interstitial sites in the sublattice of Ta_2O_5 (see Supporting Information).

Figure 4a shows the SEM image of a Ta_2O_5 nanotube after dipping it into a dilute solution of HF for 5 h. The CL spectra record from two areas of the sample labeled as A and B are shown in the insets of Figure 4a. Two peaks from the area labeled as A were detected, whereas no peak was found from the area B. The CL image under excitation at 15 kV was also measured (Figure 4b). Figure 4c shows the CL spectrum from the Ta_2O_5 nanotube sample (area A) after Gaussian fitting and reveals two clear peaks at 563 nm (2.2 eV) and 301 nm (4.1 eV), as well as a broad peak in the range of 2–5 eV. The band gap of Ta_2O_5 is about 4.1–4.2 eV, which results in some radiative recombination emission caused by oxygen deficiency.[20] The peak at 563 nm (2.2 eV) is attributed to the oxygen vacancies inside the Ta_2O_5 shell. The broad band at 2–5 eV may be derived from a combination of two peaks at 460 and 355 nm which originate from the residual SiO_2 inside the Ta_2O_5 nanotube or from the initial Si substrate. The peak at 301 nm (4.1 eV, violet region) in the CL spectrum originates from the d-band transition between the e_g and t_{2g} states, induced by

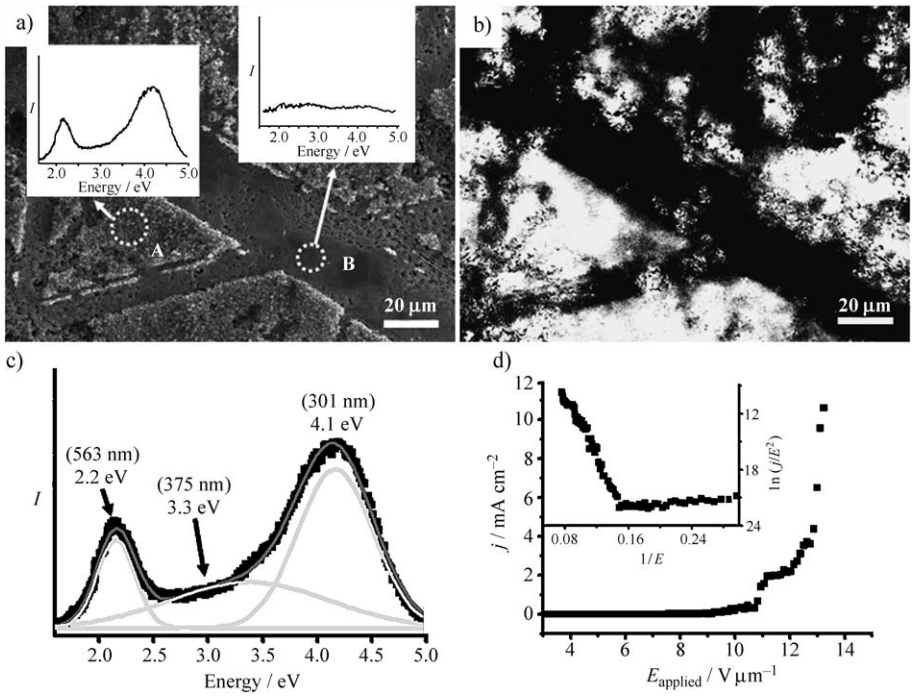

Figure 4. a) SEM image of a Ta_2O_5 nanotube after dipping it into diluted HF solution; the insets show CL spectra recorded from two areas labeled A and B. b) CL image of the sample in (a) excited at 15 kV. c) CL spectrum recorded from a Ta_2O_5 nanotube (black line) after Gaussian curve fitting (pale gray line; deconvoluted spectra are shown in dark gray). d) Field-emission properties of a Ta_2O_5 nanotube obtained from dipping a SiO_2/Ta_2O_5 core–shell structure into diluted HF solution (j = current density). The inset shows the corresponding $\ln(j/E^2)$ versus $1/E$ plot (see text for details).

ligand-field splitting (see Supporting Information).[21] A similar phenomenon is found in other materials, such as α-Fe_2O_3 nanoparticles.[22] The violet peak derived from the oxygen deficiency transition inside the Ta_2O_5 is also the factor for the CL peak at 301 nm. Violet light is of interest in fundamental research and for applications in full-color displays. Here, by controlling the thickness of the SiO_2 core inside the SiO_2/Ta_2O_5 core–shell structure, which in turn defines the CL wavelength, the nanotubes may be used in optical transportation phenomena, such as light propagation.

The current density as a function of the applied electric field for the Ta_2O_5 nanotube sample at a fixed distance of 100 μm between the anode and the surface of the nanotube is shown in Figure 4d. Two parameters, the turn-on field and the threshold field, are defined as the applied voltage (E) needed to produce a current density of 0.01 and 10 mA cm^{-2}, respectively, for which respective values of 8 and 13 V μm^{-1} were determined. The inset in Figure 4d shows a plot of $\ln(j/E^2)$ versus $1/E$. The linear relationship is consistent with the so-called Fowler–Nordheim plot (F-N plot; Figure 4d) and indicates that the field-emission behavior obeys the F-N rule, that is, electrons tunnel through the potential barrier from the conduction band to the vacuum state.[23] Although these values are somewhat higher than for other oxide materials, such as ZnO,[24] SnO_2,[2b] and $W_{18}O_{49}$,[25] the core–shell structures here still show great promise in display applications owing to their straightforward and high-yielding production and the ease with which they can be integrated in silicon-based industries.

In summary, SiO_2/Ta_2O_5 core–shell structures were synthesized by annealing SiO_2 nanowires under a reductive atmosphere of Ta at 950 °C. The morphology of the nanostructures was tunable depending on the morphology of the original SiO_2 nanowires, and the diameter of the SiO_2 nanowire inside the SiO_2/Ta_2O_5 core–shell structure could also be modified. Furthermore, Ta_2O_5 nanotubes could be prepared by removal of the template from the core—shell structures and Ta_2O_5 nanowires could be prepared directly by increasing the reduction time. The electrical and optical properties reported herein indicate that the SiO_2/Ta_2O_5 core–shell structures, Ta_2O_5 nanotubes, and Ta_2O_5 nanowires may have many interesting applications in nanotechnology.

Experimental Section

Single-crystal Si(001) wafers (resistivity: 1–30 Ω cm) were cleaned using standard cleaning procedures and then dipped in diluted HF solution (1:50 HF/H_2O) for 30 s before being loaded into the deposition system ($P > 5 \times 10^{-6}$ Torr). A 2-nm-thick layer of Au was deposited on the Si substrate at a pressure of 5×10^{-6} Torr with a deposition rate of 0.01 nm s^{-1}. Subsequently, as-deposited samples were annealed in a horizontal furnace at 1150 °C for 2 h under an atmosphere of N_2 to grow the SiO_2 nanowires. The high-density SiO_2 nanowire samples were transferred into a Ta-filament heating chamber for annealing ($P > 1 \times 10^{-6}$ Torr) at 950 °C for 12–32 h to produce SiO_2/Ta_2O_5 core–shell nanowire structures; Ta atoms were constantly vaporized from the supplementary source in this chamber (see Supporting Information). Ta_2O_5 nanotubes could be formed by dipping the core–shell structures into dilute HF solution (1:50 HF/H_2O) to remove the inner SiO_2 nanowires.

Grazing incidence X-ray diffractometry (GIXRD) with a fixed incident angle at 0.5° was carried out to identify the phases of the nanostructures. The surface morphology was examined by a field-emission scanning electron microscope (JSM-6500F) operated at 15 kV. To prepare the TEM specimen, all samples were sonicated in ethanol and then dispersed on a copper grid supported by a holey carbon film. A field-emission transmission electron microscope (JEM-3000F) operated at 300 kV, with a point-to-point resolution of 0.17 nm and equipped with an energy-dispersion spectrometer, an electron energy loss spectrometer, as well as a high-angle annular dark field detector, was used to characterize the microstructures and chemical compositions. Electron field-emission behavior was measured in a vacuum of 1×10^{-7} Torr by using a spherical stainless-steel probe (1-mm diameter) as the anode. The lowest emission current was recorded on the level of nA. The measurement distance between the anode and the emitting surface was fixed at 100 μm. The CL spectrum was measured in the scanning electron microscope with an electron probe microanalyzer (Shimadzu EPMA-1500). CL spectra were accumulated in single-shot mode within a short time of 1 s. In general, the CL excitation was performed with a beam current of about 100 nA in television scanning mode of 2.9×10^{-5} cm^2.

Received: June 3, 2006
Published online: October 20, 2006

Keywords: nanostructures · reduction · silicon · tantalum · template synthesis

[1] a) C. Yu, Q. Hao, S. Saha, L. Shi, X. Kong, Z. L. Wang, *Appl. Phys. Lett.* **2005**, *86*, 063101; b) C. S. Lao, J. Liu, P. X. Gao, L. Zhang, D. Davidovic, R. Tummala, Z. L. Wang, *Nano Lett.* **2006**, *6*, 263; c) A. B. Greytak, C. J. Barrelet, Y. Li, C. M. Lieber, *Appl. Phys. Lett.* **2005**, *87*, 151103; d) Y. L. Chueh, L. J. Chou, C. M. Hsu, S. C. Kung, *J. Phys. Chem. B* **2005**, *109*, 21831; e) Z. L. Wang, *Adv. Mater.* **2003**, *15*, 432; f) M. S. Arnold, P. Avouris, Z. W. Pan, Z. L. Wang, *J. Phys. Chem. B* **2004**, *108*, 659.

[2] a) Z. W. Pan, Z. R. Dai, Z. L. Wang, *Science* **2001**, *291*, 1947; b) P. X. Gao, Y. Ding, W. J. Mai, W. L. Hughes, C. S. Lao, Z. L. Wang, *Science* **2005**, *309*, 1700.

[3] J. H. He, T. H. Wu, C. L. Hsin, K. M. Li, L. J. Chen, Y. L. Chueh, L. J. Chou, Z. L. Wang, *Small* **2006**, *2*, 116.

[4] M. Cao, T. Liu, S. Gao, G. Sun, X. Wu, C. Hu, Z. L. Wang, *Angew. Chem.* **2005**, *117*, 4269; *Angew. Chem. Int. Ed.* **2005**, *44*, 4197.

[5] J. Zhou, Y. Ding, S. Z. Deng, L. Gong, N. S. Xu, Z. L. Wang, *Adv. Mater.* **2005**, *17*, 2107.

[6] a) Y. Zhu, F. Yu, Y. Man, Q. Tian, Y. He, N. Wu, *J. Solid State Chem.* **2005**, *178*, 224; b) H. Schulz, L. Mädler, S. E. Pratsinis, P. Burtscher, N. Moszner, *Adv. Mater.* **2005**, *17*, 830; c) A. Arranz, V. Pérez-Dieste, C. Palacio, *Phys. Rev. B* **2002**, *66*, 675420.

[7] A. M. Morales, C. M. Lieber, *Science* **1998**, *279*, 208.

[8] T. J. Trentler, K. M. Hickman, S. C. Geol, A. M. Viano, P. C. Gibbons, W. E. Buhro, *Science* **1995**, *270*, 1791.

[9] P. D. Yang, C. M. Lieber, *J. Mater. Res.* **1997**, *12*, 2981.

[10] Y. Wu, J. Xiang, C. Yang, W. Li, C. M. Lieber, *Nature* **2004**, *430*, 61.

[11] a) J. Y. Zhang, L. J. Bie, I. W. Boyd, *J. Appl. Phys.* **1998**, 37, L27; b) R. T. Webb, *Ten Years of TWT Progress Electron Power* **1985**, *2*, 120; c) S. Ezhilvalavan, T. Y. Tseng, *J. Mater. Sci. Mater. Electron.* **1999**, *10*, 9.

[12] a) D. P. Yu, Q. L. Hang, Y. Ding, H. Z. Zhang, Z. G. Bai, J. J. Wang, Y. H. Zou, W. Qian, G. C. Xiang, S. Q. Feng, *Appl. Phys. Lett.* **1998**, *73*, 3076; b) J. H. He, T. H. Wu, C. L. Hsin, L. J. Chen, Z. L. Wang, *Electrochem. Solid State Lett.* **2005**, *8*, G254.

[13] K. H. Lee, S. W. Lee, R. R. Vanfleet, W. Sigmund, *Chem. Phys. Lett.* **2003**, *376*, 498.

[14] Z. W. Pan, Z. R. Dai, C. Ma, Z. L. Wang, *J. Am. Chem. Soc.* **2002**, *124*, 1817.

[15] S. H. Li, X. F. Zhu, Y. P. Zhao, *J. Phys. Chem. B* **2005**, *108*, 17032.
[16] M. Zhang, E. Ciocan, Y. Bando, K. Wada, L. L. Cheng, P. Pirouz, *Appl. Phys. Lett.* **2002**, *80*, 491.
[17] Further details of the crystal structure investigation may be obtained from the Fachinformationszentrum Karlsruhe, 76344 Eggenstein-Leopoldshafen, Germany (fax: (+49) 7247-808-666; e-mail: crysdata@fiz-karlsruhe.de, http://www.fiz-informationsdienste.de/en/DB/icsd/depot_anforderung.html) on quoting the deposition number ICSD-43498.
[18] S. P. Murarka, *J. Vac. Sci. Technol.* **1980**, *17*, 775.
[19] S. P. Murarka, *Silicides For VULS Application*, Academic Press, New York, **1983**, p. 107.
[20] a) W. H. Knausenberger, R. N. Tauber, *J. Electrochem. Soc.* **1973**, *120*, 927; b) A. G. Revesz, J. J. Reynolds, J. F. Allison, *J. Electrochem. Soc.* **1976**, *123*, 889; c) J. Jasapara, A. V. V. Nampoothir, W. Rudolph, *Phys. Rev. B* **2001**, *63*, 045117.
[21] F. M. F. de Groot, G. Grioni, J. C. Fuggle, *Phys. Rev. B* **1989**, *40*, 5715.
[22] H. Fei, X. Ai, M. Gao, Y. Yang, T. Zhang, J. Shen, *J. Lumin.* **1996**, *66–67*, 345.
[23] a) Y. L. Chueh, L. J. Chou, S. L. Cheng, J. H. He, W. W. Wu, L. J. Chen, *Appl. Phys. Lett.* **2005**, *86*, 133112; b) Y. L. Chueh, L. J. Chou, S. L. Cheng, C. J. Tasi, *Appl. Phys. Lett.* **2005**, *87*, 223113.
[24] C. J. Lee, T. J. Lee, S. C. Lyu, Y. Zhang, H. Ruh, H. J. Lee, *Appl. Phys. Lett.* **2002**, *81*, 5048.
[25] J. Zhou, L. Gong, S. Z. Deng, J. Chen, J. C. She, N. S. Xu, R. Yang, Z. L. Wang, *Appl. Phys. Lett.* **2005**, *87*, 223108.

